Assessing the Freysoldt, Neugebauer & van de Walle (FNV) and Kumagai–Oba (KO) finite-size corrections for Ce-vacancy complexes in diamond

W. Dednam[1] **and E. B. Lombardi**[1]

[1] Research and Academic Computing: High-Performance Computing (HPC), College of Science, Engineering and Technology, University of South Africa, Tshwane, 0001, South Africa

E-mail: dednaw@unisa.ac.za

Abstract. Lanthanide-doped diamond couples the ultra wide band gap, high thermal conductivity and radiation hardness of the host with the rich electron physics of the dopant, promising solid-state qubits, single-photon emitters and spin-memory elements. Supercell density functional theory treatments of the charged Ce-vacancy complexes that underlie these functionalities suffer from spurious image–image interactions and an ill defined electrostatic zero energy; post processing finite-size corrections are therefore mandatory for quantitative defect thermodynamics.

We benchmark the two principal correction schemes – the reciprocal space potential alignment monopole method of Freysoldt, Neugebauer, van de Walle (FNV) and the real space multipole expansion of Kumagai Oba (KO) – for Ce_{V2}, Ce_{V3} and Ce_{V4} in a 216-atom diamond supercell. Uncorrected neutral formation energies agree with literature to within 0.5eV for all three and confirm Ce_{V3} as the most stable neutral complex. Introducing positive charge exposes limitations of FNV: once the anisotropic Ce $4f$ charge density departs from the isotropic monopole assumed in that formalism, FNV corrections fail to converge. In contrast, KO, which accounts for higher multipoles, remains numerically stable and delivers consistent corrections.

Our results show that KO is indispensable for heavy-atom defects with non-spherical charge distributions, while FNV is reliable only for nearly isotropic cases. This enables accurate assessment of rare-earth dopants in diamond and other wide-gap semiconductors.

1 Introduction

Doped diamond complexes are promising for spintronic [1, 2, 3, 4] and quantum optics applications [5, 6, 7, 8]. Diamond is an attractive host for these defects because it is a radiation-hard, ultra wide band gap semiconductor capable of hosting deep defect states. For example, nitrogen-doped diamond already exhibited promise towards spintronic applications in theoretical density-funtional theory (DFT) calculations in Ref. [1], and the negative nitrogen vacancy cluster has been shown to exhibit spin conherence times at room temperature up to the order of milliseconds and spin-relaxation times beyond that, which is very promising for quantum memory applications [2]. Subsequent works have continued to explore such advantageous aspects of this defect center (see Ref. [4] and references therein).

Lanthanide-doped diamond has also recently been explored for its potential, particularly in quantum optics applications. Several studies have explored Cerium [9, 10], Erbium [11, 12], Europium [5, 13, 14], Praseodymium [15, 16] and Ytterbium [11, 17] as dopants in diamond complexes of various forms.

Density-functional theory (DFT) has served as the workhorse for modelling a broad range of diamond complexes [1, 3, 15, 13, 9, 14, 18, 16, 19, 20]. However, the periodic-boundary-condition (PBC) supercell model used in DFT creates spurious electrostatic interactions between a charged defect and its periodic images, so explicit correction terms are required [21, 22, 23, 24, 25]. Conventional potential-alignment schemes give only a partial correction [22]; more sophisticated approaches (e.g. image-charge correction schemes) are needed for reliable formation energies [23, 24, 25]. In this work we assess two of these correction schemes, the *scalar* Freysoldt, Neugebauer, van de Walle (FNV) and the *tensor* Kumagai Oba (KO), and apply them to the Ce_{V2}, Ce_{V3} and Ce_{V4} complexes of diamond studied in Ref. [9].

2 Methods

The FNV and KO finite-size corrections outlined below follow their implementation in the `SPINNEY` post-processing code, with conventions as defined by Ref. [26]. The formation energy of a charged defect supercell in DFT is conventionally defined as [26]:

$$E_f\big[D^q\big] = \big\{E\big[D^q\big] + E_{\mathrm{corr}}\big[D^q\big]\big\} - E_P - \sum_i n_i\mu_i + q(\varepsilon_{\mathrm{VBM}} + \Delta\varepsilon_F)\,. \tag{1}$$

where $E_f\big[D^q\big]$ is the ground-state DFT total energy of the defect supercell in charge state q and E_P is the neutral pristine diamond supercell. n_i is the number of removed (<0) or added (>0) atoms and μ_i is the chemical potential of atom type i. E_{VBM} is the valence-band maximum (VBM) of the pristine supercell. $\Delta\varepsilon_F$ is the Fermi level relative to the VBM. Finally, $E_{\mathrm{corr}}\big[D^q\big]$ consists of two terms: the image-charge correction and potential alignment.

Under PBC, a charged defect interacts with its own periodic images and the neutralising background ($\frac{-q}{\Omega}$, with Ω the supercell volume). Image-charge corrections remove this artificial long-range interaction, so that $E_f\big[D^q\big]$ converges toward the dilute-defect limit in the ideal case [25]. A potential alignment correction is also needed since the DFT Poisson solver sets the cell-average potential $V_{\mathrm{avg},\Omega}$ to zero arbitrarily [25]. The charged cells inherit this potential shift, which, in turn, alters Kohn-Sham eigenvalues and total energies.

The FNV method defines the correction terms as [26]:

$$E_{\mathrm{corr}}\big[D^q\big] = -\,E_{\mathrm{model}} - q\,\Delta V_{\mathrm{model},\,q/b}\big|_{\mathrm{far}} \tag{2}$$

where E_{model} is the electrostatic (Madelung) energy of a model charge density, which can be a point charge (PC) or a charge density fitted to a suitable (radially isotropic) function. $\Delta V_{\mathrm{model},\,q/b}\big|_{\mathrm{far}}$ is the value of $\Delta V_{\mathrm{model},\,q/b}$, the difference between the defect-induced potential $V_{q/b}$ and the and the charge-density model potential $V_{\mathrm{model},q}$ far away from the defect inside Ω. For convenience, the overall correction term in Eq. (1) has traditionally been analyzed in Ewald summation form divided into real and reciprocal space parts [21, 25]. The electrostatic component of this correction can thus be defined as [25, 26]:

$$E_{\mathrm{model}} = \frac{1}{2\,\varepsilon\,\Omega}\sum_{\mathbf{G}\neq\mathbf{0}}\frac{4\pi}{|\mathbf{G}|^2}\left|\tilde{\rho}_{\mathrm{model,d}}(\mathbf{G})\right|^2 \;-\; \frac{1}{\pi\,\varepsilon}\int_0^\infty \kappa\left|\tilde{\rho}_{\mathrm{model,d}}(\kappa)\right|^2 d\kappa, \tag{3}$$

where $\tilde{\rho}_{\mathrm{model,d}}(\mathbf{G}) = \int_\Omega \rho_{\mathrm{model,d}}(\mathbf{r})\,e^{-i\mathbf{G}\cdot\mathbf{r}}\,d^3r$, $\kappa = |\mathbf{G}|$, and ε is the dielectric constant of the relaxed defect supercell calculated within the linear response regime in our DFT calculations. The first term of Eq. (3) is just the Fourier transform of the electrostatic energy of $\rho_{\mathrm{model,d}}$ and the second term corrects for the self-energy of an isolated charge density [25]. The model charge density is defined as [23, 26]:

$$\rho_{\mathrm{model,d}}(\mathbf{r}) = qx\,\frac{e^{-|\mathbf{r}-\mathbf{r}_0|/\gamma}}{N_\gamma} + q(1-x)\,\frac{e^{-|\mathbf{r}-\mathbf{r}_0|^2/\beta^2}}{N_\beta}, \tag{4}$$

where $N_\gamma = 8\pi\,\gamma^3$, $N_\beta = \pi^{3/2}\,\beta^3$, and x, β and γ are fitting parameters with $\mathbf{r}_0$ is centered on the defect [23, 24, 25]. Equation (4) represents a weighted sum of an exponentially decaying radial charge distribution and a localised Gaussian charge distribution. If the weighting factor $x = 1$, then the model charge density is completely delocalised, with the opposite case occurring when $x = 0$: the charge density is fully localised.

Importantly, the potential alignment $\Delta V_{\mathrm{model},\,q/b}\big|_{\mathrm{far}}$ in the FNV correction varies strongly around the defect as the extent of relaxation of atoms around it increases [24, 25]. A planar average of this potential is used in the FNV correction [23, 26]. Hence, relaxation of atoms at the defect gives rise to an anisotropic charge distribution which the scalar FNV correction may not be able to accurately capture [24, 25].

To remedy this inherit deficiency, the *tensor* KO extension of the *scalar* FNV correction was introduced [25]:

$$E_{\mathrm{corr}}\big[D^q\big] = -\,E_{\mathrm{PC}} - q\,\Delta V_{\mathrm{PC,q/b}} \tag{5}$$

$$E_{\rm PC} = \frac{1}{2\Omega} \sum_{\mathbf{G}\neq\mathbf{0}} \frac{4\pi}{\mathbf{G}^{\rm T}\varepsilon\,\mathbf{G}} \left|\tilde{\rho}_{\rm model,d}(\mathbf{G})\right|^2 = \frac{2\pi q^2}{\Omega} \sum_{\mathbf{G}\neq\mathbf{0}} \frac{1}{\mathbf{G}^{\rm T}\varepsilon\,\mathbf{G}} \tag{6}$$

$$\tilde{\rho}_{\rm model,d}(\mathbf{G}) = \int_\Omega \rho_{\rm model,d}(\mathbf{r})\, e^{-i\mathbf{G}\mathbf{r}}\, d^3r = \int_\Omega q\,\delta(\mathbf{r}-\mathbf{r}_0)\, e^{-i\mathbf{G}\mathbf{r}}\, d^3r = q, \tag{7}$$

where now ε is the dielectric *tensor* also obtained from a DFT linear response calculation on the relaxed defect supercell. In practice, ε is diagonalized and both ε and $\mathbf{G}$ are rotated into the principal-axis frame (where ε is diagonal), so that $\mathbf{G}^{\rm T}\varepsilon\,\mathbf{G} = \sum_i \varepsilon_i\, G_i^2$ [25]. Note that here the constant (and divergent) electrostatic self-interaction term cancels exactly in Eq. (5) because it appears with the same magnitude but opposite sign in the electrostatic energy $E_{\rm PC}$ and the reference potential $V_{\rm PC}$ used to define the alignment term $\Delta V^{\rm far}_{\rm PC,q/b}$ in the KO scheme [25]. Hence, no explicit self-energy contribution is needed when Eq. (5) is used in Eq. (1).

Figure 1 shows the Ce-vacancy complexes considered in this work: Ce inserted into a divacancy, a trivacancy or at the site of 4 C atoms removed. They have been created from a relaxed 216-atom diamond supercell with lattice constant 3.574 Å, in close analogy with the structures employed in Ref. [9]. [1]

We performed DFT calculations in `CASTEP` [27] on the input structures, which were randomly distorted from ideal symmetry to ensure energetically most favorable final structures after optimization, using on-the-fly-generated (OTFG) ultra-soft pseudopotentials [28]. An energy cutoff of 540 eV and a $3 \times 3 \times 3$ reciprocal-space sampling k-mesh were employed. To account for localisation of the $4f$ orbitals on Ce, we used PBE+U [29, 30] with the default value of $U = 6.0$ eV for Ce in CASTEP. The same range of initial charge states as in Ref. [9] were used: $q = -1, 0, +1, +2, +3, +4$. In addition, to be able to account for all possible defect spin states, different initial spin states for each charge state were considered: $0, 1, 2, ..., 6, 7$. The structures were relaxed to tolerance 0.01 eV/Å. [2]

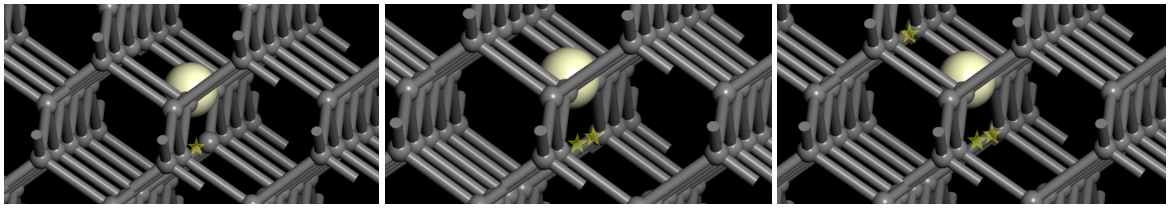

Figure 1: The initial (*left*) $\mathrm{Ce_{V2}}$, (*middle*) $\mathrm{Ce_{V3}}$ and (*right*) $\mathrm{Ce_{V4}}$ complexes used in this work. Faded yellow stars indicate the nearest-neighbour atoms of Ce that have been removed by analogy with Ref. [9].

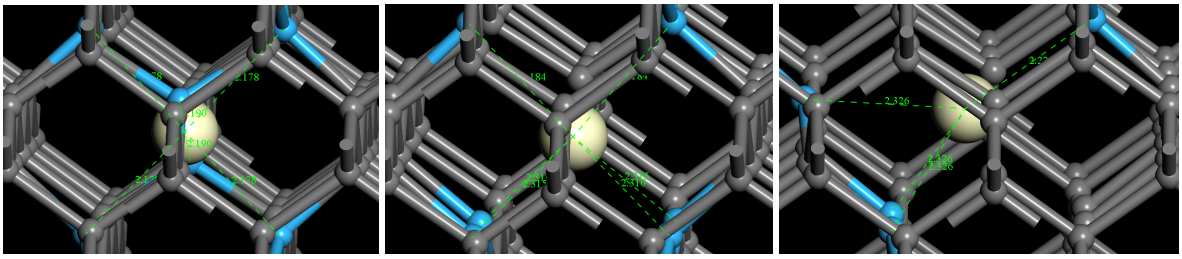

Figure 2: The optimized (*left*) $\mathrm{Ce_{V2}}$, (*middle*) $\mathrm{Ce_{V3}}$ and (*right*) $\mathrm{Ce_{V4}}$ complexes. The dopant and nearest-neighbour (nn) carbon atoms within the second nn shell of pristine diamond are shown. The bond distances are also shown. In $\mathrm{Ce_{V2}}$, all six nearest neighbours are ≈ 2.2 Å from the Ce atom. In $\mathrm{Ce_{V3}}$, two nearest neighbours are ≈ 2.2 Å, and the other four ≈ 2.3 Å, from the Ce atom. In $\mathrm{Ce_{V4}}$, one nearest neighbour is ≈ 2.2 Å, and the other three ≈ 2.3 Å, from the Ce atom. All other carbon atoms are further than the second nn shell of pristine diamond (2.53 Å) from the Ce atom.

[1] We use a different naming convention for our Ce-vacancy complexes because the Ce atoms do not remain at substitutional sites after relaxation, as implied by the naming convention of Ref. [9]: CeV, CeV2 and CeV3.

[2] The `CASTEP` utility `c2x` was employed to convert output binary files to Gaussian `cube` format read by `SPINNEY`.

3 Results

The relaxed vacancy complexes are shown in Fig. 2. The dopant and nearest neighbour carbon atoms within the second-nearest neighbour shell of pristine diamond (2.53 Å) are highlighted. The extent of coordination and the increasing disparity between neighbouring bond lengths indicate the growing disorder about the relaxed point defects.

It should not come as a surprise that the FNV corrections become increasingly unreliable as the disorder about the dopant increases [25]. This can be seen by comparing the obtained overall FNV and KO corrections (in eV) in tables 1–3. We also calculated the enclosed charge within each supercell based on the fitting parameters x, β and γ obtained from Eq. (4) during the FNV correction calculation. Then, to enable a comparison with the conventional potential alignment term in the second-to-last column, the FNV and KO potential alignment terms are also listed. To obtain the conventional values, we compared the electrostatic potential of the defect supercells at an interstitial centroid far away from the defect with that of the relaxed pristine supercell at the same location.

q	$S_{\min}$	FNV total	FNV ΔV_{far}	KO total (eV)	KO ΔV_{far}	Conventional ΔV	q_{enc}
-1	0.98754	0.226	0.118	0.217	0.126	0.163	-0.99999996
0	0.0000022	0.0	-0.003	0.0	0.001	0.0	0.0
$+1$	1.0007	0.205	-0.119	0.210	-0.114	-0.157	0.99999994
$+2$	2.00004	0.774	-0.222	0.771	-0.222	-0.303	1.9999998
$+3$	2.08479	1.893	-0.346	1.796	-0.345	-0.3134	2.9999994
$+4$	2.17017	27.245	-0.098	0.865	-0.087	-0.3365	3.9998

Table 1: FNV and KO total correction and potential alignment values (eV) for vacancy complex Ce_{V2}. $S_{\min}$ corresponds to the spin state of lowest total energy. The conventional potential alignment is included for comparison. The enclosed charge within each supercell is calculated as $q_{\text{enc}}(r) = 4\pi \int_0^r \rho_{\text{model,d}}(r')\, r'^2\, dr'$ with $\rho_{\text{model,d}}$ as defined in Eq. (4) and the integration performed on interval $0 < r \leq \frac{1}{2} L_{\min}$ with $L_{\min} = \min_i \|\mathbf{a}_i\|$ and $\mathbf{a}_i$ the supercell side lengths.

q	$S_{\min}$	FNV total	FNV ΔV_{far}	KO total (eV)	KO ΔV_{far}	Conventional ΔV	q_{enc}
-1	1.0	0.317	0.113	0.202	0.116	0.121	-0.9999995
0	0.0019	0.0	-0.003	0.0	0.003	0.0	0.0
$+1$	0.99811	297.953	297.953	0.201	-0.102	-0.134	7.3×10^{-6}
$+2$	0.00062	1498.712	749.356	0.725	-0.197	-0.227	9.2×10^{-6}
$+3$	0.787866	2967.798	989.266	1.415	-0.268	-0.288	1.4×10^{-5}
$+4$	0.188895	3526.123	881.531	1.712	-0.234	-0.345	1.8×10^{-5}

Table 2: FNV and KO total correction and potential alignment values (eV) for vacancy complex Ce_{V3}. The meanings of the remaining columns carry over from table 1.

q	$S_{\min}$	FNV total	FNV ΔV_{far}	KO total (eV)	KO ΔV_{far}	Conventional ΔV	q_{enc}
-1	1.0	292.236	-292.236	0.147	0.079	0.119	-4.6×10^{-6}
0	0.0	0.0	-0.001	0.0	0.001	0.0	0.0
$+1$	0.990084	285.872	285.872	0.186	-0.104	-0.122	7.3×10^{-6}
$+2$	0.00087	1113.150	556.575	0.727	-0.202	-0.237	1.4×10^{-5}
$+3$	0.961946	2218.033	739.344	1.450	-0.268	-0.322	2.2×10^{-5}
$+4$	0.337866	2843.334	710.833	1.886	-0.252	-0.392	2.9×10^{-5}

Table 3: FNV and KO total correction and potential alignment values (eV) for vacancy complex Ce_{V4}. The meanings of the remaining columns carry over from table 1.

With the exception of charge state $q = +4$, $\mathrm{Ce_{V2}}$ in table 1 exhibits consistent values of the total FNV and KO corrections. The potential alignments of the two schemes also agree and both agree reasonably well with the conventional scheme. For the $q = +3$ charge state, possible metastable spin states have been found; only the most stable spin states are reported: $S_{\min}$ corresponds to the spin state of lowest total energy. The other spin-state total energies of $q = +3$ differ from the minimum by at most 6.0×10^{-5} eV. Hence, given this small value, we conclude that there are no metastable spin states for this vacancy complex. Finally, the FNV model charge calculated from Eq. (4) for each defect supercell agrees with the charge state specified in the CASTEP calculation. The discrepancy between the FNV and KO corrections for charge state $q = +4$ suggests that it is highly anisotropic. This is an example of the inherit deficiency in the FNV method that the KO correction was meant to overcome[25].

We immediately observe how the situation changes when we consider the next vacancy complex with increased disorder: $\mathrm{Ce_{V3}}$. FNV only yields reasonable total correction and potential alignment values for the $q = -1$ charge state. The FNV model charge enclosed in the supercell also tallies with this charge. The FNV correction and potential alignment values blow up for all positive charge states, and the fact that the essentially zero fitted charge densities do not agree with them suggests that the charge is delocalised, and that these defects are shallow, unlike the localised deep states in $\mathrm{Ce_{V2}}$. For $q = 0$, all non-zero initial spin states turn out to be metastable, with total energies that differ by up to ≈ 0.01 eV from $S_{\min}$. These energetically less favourable spin states have $S \approx 2.0$ compared to $S_{\min} \approx 0.002$.

For the largest and most disordered vacancy cluster, $\mathrm{Ce_{V4}}$, the FNV correction fails across the board, and all non-zero charge states yield shallow defects with the FNV model charge delocalised beyond the confines of a single defect supercell. The total energy difference between metastable spin states (for a given charge state) is up to ≈ 0.05 eV for $q = +2$. The less energetically favourable spin states all end up as $S \approx 2.0$ whilst $S_{\min} \approx 1 \times 10^{-5}$. In constrast to $q = +4$ of $\mathrm{Ce_{V2}}$, the FNV correction ultimately fails here not because the defect is anisotropic but rather because it is shallow, as is evident from the delocalised model charge in the last columns of tables 2 and 3.

The KO correction, on the other hand, delivers consistent values across all charge states. This is to be expected given that it employs a point-charge electrostatic and atomic-site potential alignment model which by design cannot discern the spatial extent of the charge distribution. Where KO agrees with the FNV correction, we know that we are dealing with deep defect states

Finally, it is worth mentioning that the stability of the neutral vacancy complexes in our work follows the same trend as the relaxed defects in Refs. [9, 16]: $E_f\big[D^0\big]_{\mathrm{Ce_{V2}}} = 15.5259$ eV, $E_f\big[D^0\big]_{\mathrm{Ce_{V3}}} = 14.3588$ eV and $E_f\big[D^0\big]_{\mathrm{Ce_{V4}}} = 14.5393$ eV. In other words, the neutral $\mathrm{Ce_{V3}}$ complex is the most stable.

In conclusion, the FNV and KO correction schemes have been evaluated for a set of three Ce-vacancy complexes across various charge states, and spin states for each charge. The FNV correction fails gracefully in the presence of a shallow defect whilst the KO correction continues to provide reasonable values. FNV results in unrealistically large correction values for shallow levels, allowing defects with shallow levels to be identified. Ultimately, the cure for a failing FNV correction is to employ hybrid exchange-correlation functionals as is our intention in future work.

References

[1] E. B. Lombardi, A. Mainwood, K. Osuch, and E. C. Reynhardt, "Computational models of the single substitutional nitrogen atom in diamond," *J. Phys. Condens. Matter*, vol. 15, no. 19, pp. 3135–3149, 2003.

[2] N. Zhao, J.-L. Hu, S.-W. Ho, J. T. K. Wan, and R. B. Liu, "Atomic-scale magnetometry of distant nuclear spin clusters via nitrogen-vacancy spin in diamond," *Nat. Nanotechnol*, vol. 6, no. 4, pp. 242–246, April 2011.

[3] E. M. Benecha and E. B. Lombardi, "Cu doped diamond: Effect of charge state and defect aggregation on spin interactions in a 3 d transition metal doped wide band-gap semiconductor," *J. Appl. Phys.*, vol. 123, no. 18, p. 185706, 2018.

[4] M. Gulka, D. Wirtitsch, V. Ivády, J. Vodnik, J. Hruby, G. Magchiels, E. Bourgeois, A. Gali, M. Trupke, and M. Nesladek, "Room-temperature control and electrical readout of individual nitrogen-vacancy nuclear spins," *Nat. Commun.*, vol. 12, no. 1, pp. 1–8, 2021.

[5] A. Magyar, W. Hu, T. Shanley, M. E. Flatté, E. Hu, and I. Aharonovich, "Synthesis of luminescent europium defects in diamond," *Nat. Commun.*, vol. 5, pp. 1–6, 2014.

[6] V. S. Sedov and E. al., "Diamond-EuF3 nanocomposites with bright orange photoluminescence," *Diam. Relat. Mater.*, vol. 72, pp. 47–52, 2017.

[7] P. Rembold, N. Oshnik, M. M. Müller, S. Montangero, T. Calarco, and E. Neu, "Introduction to quantum optimal control for quantum sensing with nitrogen-vacancy centers in diamond," *AVS Quantum Science*, vol. 2, no. 2, 2020.

[8] V. Sedov, S. Kuznetsov, A. Martyanov, and V. Ralchenko, "Luminescent diamond composites," *Funct. diam.*, vol. 2, no. 1, pp. 53–63, 2022. [Online]. Available: https://doi.org/10.1080/26941112.2022.2071112

[9] X. Tan, X. Wei, L. Chen, and Z. Liu, "Study of the structural stability and electronic structure of Ce-related defects in diamonds," *Opt. Mater. Express*, vol. 10, no. 5, p. 1286, 2020.
[10] X. Tan, J. Wang, X. Wei, C. Pan, Y. Ren, S. Sun, and H. Jia, "First-principle study on the influence of common impurities in diamond on the electronic structure of Ce-related defects," *Opt. Mater. Express*, vol. 11, no. 10, p. 3421, 2021.
[11] J. Cajzl, B. Akhetova, P. Nekvindová, A. Macková, P. Malinský, J. Oswald, Z. Remeš, M. Varga, and A. Kromka, "Co-implantation of Er and Yb ions into single-crystalline and nano-crystalline diamond," *SIA*, vol. 50, no. 11, pp. 1218–1223, 2018.
[12] D. Propst, J. Kotakoski, and E. H. Åhlgren, "Impurity atom configurations in diamond and their visibility via scanning transmission electron microscopy imaging," *EST*, vol. 5, no. 3, 2023.
[13] D. E. Vanpoucke, S. S. Nicley, J. Raymakers, W. Maes, and K. Haenen, "Can europium atoms form luminescent centres in diamond: A combined theoretical–experimental study," *Diam. Relat. Mater.*, vol. 94, no. February, pp. 233–241, 2019.
[14] X. Tan, Z. Liu, Z. Liu, Y. Ren, S. Sun, and H. JIa, "Principle study of the europium vacancy color center in a diamond," *Opt. Mater. Express*, vol. 10, no. 12, p. 3277, 2020.
[15] X. Tan, T. Liu, X. Liu, Y. Ren, S. Sun, H. Jia, Z. Liu, L. Chen, and X. Wei, "Structural stability of Pr-related defects in diamond and electronic structure single photon source: A first-principles study," *AIP Advances*, vol. 8, no. 10, p. 105202, 2018.
[16] I. M. Morris, K. Klink, J. T. Singh, J. L. Mendoza-Cortes, S. S. Nicley, and J. N. Becker, "Rare isotope-containing diamond colour centres for fundamental symmetry tests," *Phil. Trans. R. Soc. A*, vol. 382, no. 2265, 2024.
[17] D. G. Babar, J. Nuwad, S. K. Agarwalla, D. Jain, G. Sridhar, and V. Sudarsan, "Enhancing Luminescence Properties of Lab-Grown Diamond Films with Upconversion Nanoparticles for High-Performance Surface Temperature Sensing in Advanced Applications," *ACS Appl. Opt. Mater.*, vol. 2, no. 8, pp. 1546–1558, 2024.
[18] J. Cajzl, P. Nekvindová, A. Macková, M. Varga, and A. Kromka, "Erbium ion implantation into LiNbO3, Al2O3, ZnO and diamond - measurement and modelling - an overview," *Phys. Chem. Chem. Phys.*, vol. 24, no. 32, pp. 19 052–19 072, 2022.
[19] N. Ghafari Cherati, A. Pershin, and Á. Gali, "Sulfur in diamond and its effect on the creation of nitrogen-vacancy defect from ab initio simulations," *Phys. Rev. Research*, vol. 7, no. 1, p. 13278, 2025.
[20] Z. Wang, P. Jin, P. Qu, F. Cao, X. Han, and Z. Wang, "Progress in first-principles studies on doped semiconductor diamond," *EPJ ST*, vol. 123, 2025.
[21] G. Makov and M. C. Payne, "Periodic boundary conditions in ab initio calculations," *Phys. Rev. B*, vol. 51, no. 7, pp. 4014–4022, 1995.
[22] S. Lany and A. Zunger, "Assessment of correction methods for the band-gap problem and for finite-size effects in supercell defect calculations: Case studies for ZnO and GaAs," *Phys. Rev. B*, vol. 78, no. 23, pp. 17–20, 2008.
[23] C. Freysoldt, J. Neugebauer, and C. G. Van De Walle, "Fully Ab initio finite-size corrections for charged-defect supercell calculations," *Phys. Rev. Lett.*, vol. 102, no. 1, pp. 1–4, 2009.
[24] H. P. Komsa, T. T. Rantala, and A. Pasquarello, "Finite-size supercell correction schemes for charged defect calculations," *Phys. Rev. B*, vol. 86, no. 4, pp. 1–16, 2012.
[25] Y. Kumagai and F. Oba, "Electrostatics-based finite-size corrections for first-principles point defect calculations," *Phys. Rev. B*, vol. 89, no. 19, 2014.
[26] M. Arrigoni and G. K. Madsen, "Spinney: Post-processing of first-principles calculations of point defects in semiconductors with Python," *Comput. Phys. Commun.*, vol. 264, p. 107946, 2021.
[27] S. J. Clark, M. D. Segall, C. J. Pickard, P. J. Hasnip, M. I. J. Probert, K. Refson, and M. C. Payne, "First principles methods using CASTEP," *Z. Kristallogr. Cryst. Mater*, vol. 220, no. 5/6, pp. 567–570, 2005.
[28] D. Vanderbilt, "Soft self-consistent pseudopotentials in a generalized eigenvalue formalism," *Phys. Rev. B*, no. 11, pp. 7892–7895, apr 1990.
[29] J. P. Perdew, K. Burke, and M. Ernzerhof, "Generalized gradient approximation made simple," *Phys. Rev. Lett.*, vol. 77, no. 18, pp. 3865–3868, oct 1996.
[30] S. L. Dudarev, G. A. Botton, S. Y. Savrasov, C. J. Humphreys, and A. P. Sutton, "Electron-energy-loss spectra and the structural stability of nickel oxide: An lsda+u study," *Phys. Rev. B*, vol. 57, pp. 1505–1509, Jan 1998.